Solar Energy 209 (2020) 662–673

Contents lists available at ScienceDirect

Solar Energy

journal homepage: www.elsevier.com/locate/solener

Effects of retro-reflective and angular-selective retro-reflective materials on solar energy in urban canyons

Mattia Manni [a], Marta Cardinali [a], Gabriele Lobaccaro [b,*], Francesco Goia [c], Andrea Nicolini [a,d], Federico Rossi [a,d]

[a] CIRIAF – Interuniversity Research Center on Pollution and Environment "Mauro Felli", Perugia, Italy
[b] Department of Civil and Environmental Engineering, Faculty of Engineering, Norwegian University of Science and Technology NTNU, Trondheim, Norway
[c] Department of Architecture and Technology, Faculty of Architecture and Design, Norwegian University of Science and Technology NTNU, Trondheim, Norway
[d] Department of Engineering, University of Perugia, Perugia, Italy

ARTICLE INFO

Keywords:
Retro-reflective materials
Angular-selective retro-reflective materials
Solar accessibility
Urban canyon modelling

ABSTRACT

The study deals with the application of retro-reflective (RR) and angular-selective retro-reflective (AS-RR) coatings on surfaces (i.e. the street ground and the south-exposed façade) within the urban canyon. Solar analyses were conducted at different latitudes (Oslo, Milan, and Cairo) by varying the urban canyon height-to-width ratio (H/W) to determine the variation in solar irradiation absorbed by north and south façades. Both summer and winter conditions were considered, and up to five material patterns (one reference case and four enhanced scenarios) were investigated for each combination of latitude and height-to-width ratio values. A validated Monte Carlo-based numerical model was used to conduct full-ray tracing analyses and to simulate the behavior of these coatings. The outcomes allowed the development of guidelines for the adoptions of RR and AS-RR materials in different scenarios. It was demonstrated that RR and AS-RR materials applied to the street performed better in low-density urban environment ($H/W \leq 0.5$) with a consequent increase of the solar energy gains on the north façade by up to 15%. Employing RR and AS-RR materials on the south-exposed façade showed greater effectiveness on high-density urban canyon ($H/W \geq 2.0$) and reduced by up to −8% the solar irradiation absorbed by the façade.

1. Introduction

Urban morphology and materials properties play a relevant role in assuring a healthy and comfortable living environment (Santamouris et al., 2015; Zhou et al., 2016), especially because the recent growth of the population living in cities has caused an increase in the densification of the urban pattern (United Nations, 2014). Such a growth can lead to several climate-related issues amongst which the most documented is the so-called Urban Heat Island (UHI) effect (Rahman et al., 2017; Xu et al., 2018). The main causes of this phenomenon are found in the lack of permeable and vegetated surfaces, the materials used in the built environment, the anthropogenic heat, the worsened ventilation within urban canopies, and the higher pollutants concentration in the atmosphere (Oke, 1981; Piselli et al., 2018; Warren, 2014; Xie et al., 2005). Documented issues linked to the UHI effect are related to increase of energy use for cooling of buildings (Pantavou et al., 2013), worsening of human health, and pedestrian thermal stress (Pioppi et al., 2020). Such consequences are more evident within urban canyons (UC), which consist of street corridors defined by the height-to-width ratio (H/W) parameter (named "aspect ratio" from here on) where the height (H) is the average of the buildings' height and the width (W) refers to the street (i.e. the distance between the opposite façades facing the canyon).

Several studies focused on mitigation strategies through green infrastructures (e.g. urban park, tree lined street) and identified implementing evapotranspiration from plants (Grilo et al., 2020; Lobaccaro et al., 2019; Ziaul and Pal, 2020), creating blue infrastructure (i.e. bodies of water) (Battista et al., 2019), increasing energy storage potential (Kousis et al., 2020; Piselli et al., 2019), and applying cool materials (i.e. high-reflective coatings) on urban surfaces (i.e. terrain, façades and roofs) (Liu and Morawska, 2020; Manni et al., 2020b) as the most effective measures. Surface treatments and building coatings are demonstrated to impact on the urban microclimate, hence exploiting materials with a high solar reflectance in the visible range and high infra-red (IR) emissivity allows one reducing surface and air temperatures, lowering both energy use for cooling and electricity energy peaks,

* Corresponding author.
E-mail address: gabriele.lobaccaro@ntnu.no (G. Lobaccaro).

https://doi.org/10.1016/j.solener.2020.08.085
Received 7 July 2020; Received in revised form 21 August 2020; Accepted 27 August 2020

Nomenclature and acronyms

Variables

Irr	solar irradiation
H/W	height-to-width ratio
H	height
W	width
max	maximum values
min	minimum values
ab	ambient bounces

Greek letters

Δ	variation

Subscripts

dir	direct
hor	horizontal
abs	absorbed
ref	reference case
enh	enhanced scenario
sum	summer conditions
win	winter conditions
%	percentage
wt	weighted

Acronyms

UHI	urban heat island
UC	urban canyon
IR	infra-red
HR	high-reflective
RR	retro-reflective
AS-RR	angular-selective retro-reflective
TMY	typical meteorological year
FE	finite element

and improving indoor comfort conditions (Jandaghian and Berardi, 2020). Nonetheless, when applied to building façade, their effectiveness is negatively influenced by factors such as urban density and window-to-wall ratio (Nazarian et al., 2019).

High-reflective (HR) materials also presented some drawbacks in relation to solar energy gains through building envelope during winter, leading to the increase of the energy use for heating, and the progressive decrease of albedo value due to aging, pollution, and weathering effects (Tsoka et al., 2018). These effects occurred because cool materials generally reflect most of the solar irradiation in a diffuse way and this may contribute to exacerbate the UHI phenomenon by increasing the amount of multiple and mutual inter-buildings reflections (particularly when it comes to high dense built environments), while reducing the absorbed fraction. To overcome this issue, retro-reflective (RR) materials were proposed as innovative coatings capable of reflecting backward the solar irradiation. Such a behavior is more evident when sunrays hit the RR surface perpendicularly, while for higher and lower angles of incidence the RR properties progressively decrease, and specular and diffuse reflections are observed (Rossi et al., 2015). Compared to HR materials, RR materials decrease the occurrence of multiple reflections within the urban canyon by directly reflecting solar irradiation towards the skydome.

Despite the advantages in the applications of RR materials, a pitfall of such a strategy is that they reduce the useful solar gains during the winter season (Mauri et al., 2018; Vallati et al., 2018). For this reason, the development of a selective behavior on RR materials represents a fundamental step to enable more effective cool materials capable of showing an optimized performance across the different seasons (Manni et al., 2018). The concept behind the angular-selective retro-reflective (AS-RR) materials is to have surface treatments capable of providing a selective response depending on the angle of incidence of the solar radiation. This behavior enables high solar gains during winter when the azimuth of sunrays is lower, and high reflection of the solar irradiation outside the urban canyon during summer when the azimuth of sunrays is higher. Some concepts of selective RR materials have recently been proposed (Sakai and Iyota, 2017) along with methodologies to define their angular range of activation (Manni et al., 2018; Zinzi et al., 2015). However, the impact of AS-RR materials on urban microclimates and mutual solar reflections between buildings has only been investigated in preliminary studies (Manni et al., 2019).

The aim of the present study is to investigate the potential applications of RR and AS-RR materials on the street ground and the south-exposed façade, that is the most irradiated surface according to (Lobaccaro et al., 2018), and their influences on the solar gains considering all the façades of the UC. This study has the ambition to contribute to a better understanding of the effects of RR and AS-RR

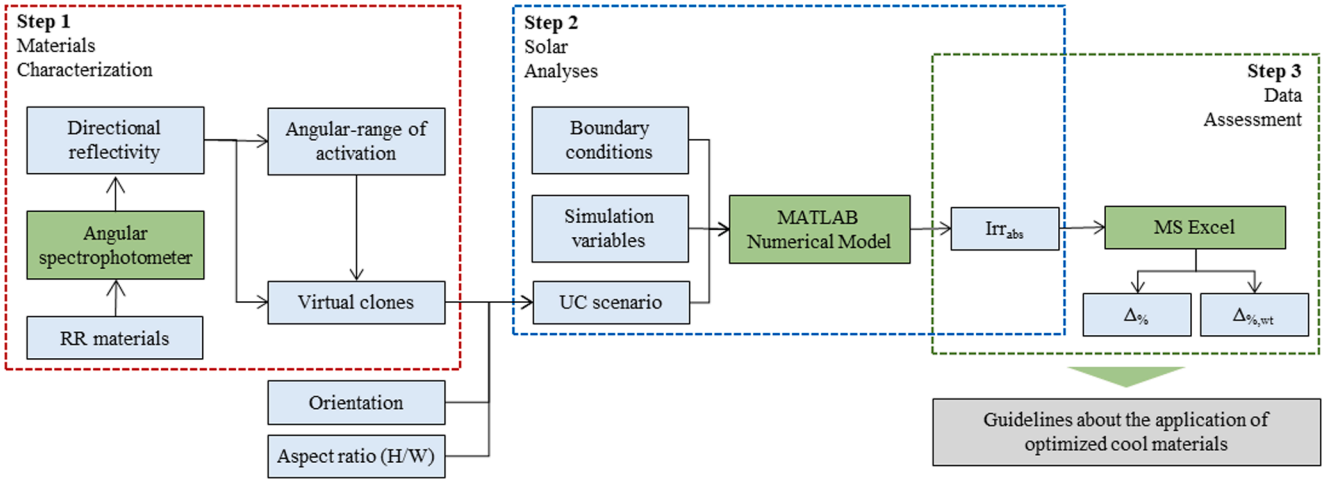

Fig. 1. Overview of the workflow. The green boxes indicate the utilized tools, the light blue ones refer to input and output parameters, the main research outcomes are reported in the grey box. For the described colours, please see the digital version. (For interpretation of the references to colour in this figure legend, the reader is referred to the web version of this article.)

Table 1
Coefficients describing the material reflective properties depending on the angle of incidence of the solar irradiation.

	Angle of incidence								
	0–10°	10–20°	20–30°	30–40°	40–50°	50–60°	60–70°	70–80°	80–90°
Retro-reflection coefficient	0.13	0.10	0.14	0.13	0.09	0.15	0.16	0.14	0.00
Diffuse reflection coefficient	0.27	0.27	0.25	0.26	0.27	0.25	0.22	0.24	0.40
Specular reflection coefficient	0.00	0.03	0.01	0.01	0.03	0.00	0.02	0.03	0.00

materials on urban microclimate by conducting solar analyses for various urban density patterns in different climate zones (Southern zone, Central zone, and Northern zone).

This work takes the move from the AS-RR materials conceptualized in (Manni et al., 2018), and later developed in (Manni et al., 2019), by defining guidelines about their exploitation as innovative urban coatings (i.e. building façade, street ground) through the Monte Carlo-based numerical model validated in (Manni et al., 2020a). The effectiveness of the angular ranges of activation of the RR properties identified in (Manni et al., 2018) is also addressed by the present study.

The paper is structured as follows. The *Methods and materials* section (Section 2) is articulated around three sub-sections describing the main steps of the workflow (Sections 2.1–2.3). The *Result and Discussion* section (Section 3) reports the simulation outcomes for the reference case (Section 3.1) and for the different enhanced scenarios (Section 3.2), and analyses them for each climate zone, before a cluster of guidelines is determined (Section 3.3) and limitations are highlighted (Section 3.4). Finally, the *Conclusions and future developments* section summarizes the knowlegde generated and the implications of this work (Section 4).

2. Methods and materials

The influences of RR and AS-RR materials on solar irradiation absorbed by building façades are assessed by using the numerical model developed in a previous study (Manni et al., 2020a). The workflow is arranged into three steps (Fig. 1) from materials characterization (*Step 1*) to solar analyses (*Step 2*), and to data assessment (*Step 3*). These steps are described in the following sections.

2.1. Step 1: From material characterization to the virtual clones

In *Step 1*, the RR materials were characterized. The spatial distribution of the reflected irradiation was analyzed for various angles of incidence of the sunrays. Then, AS-RR coatings were modeled by applying the angular ranges of activation identified in a previous part of this research (Manni et al., 2018) to the RR materials previously characterized. The virtual clones of the materials were finally generated and utilized together with the aspect ratio and the orientation parameters to determine the investigated UC scenarios.

The RR materials consisted of barium titanate glass microspheres and they were characterized in (Castellani et al., 2017). The directional response of such materials was assessed through a dedicated experimental test rig, which is described in (Rossi et al., 2015). It is composed by (i) an artificial solar radiation source, (ii) an inclined plane to test various exposures of the sample (i.e. various angles of incidence), (iii) 19 photodiodes arranged on a semi-cylinder every 10° degrees (from −90° to 90°, with the null value corresponding to the direction perpendicular to the plane of incidence), and (iv) a data acquisition system. The campaign for material characterization demonstrated that such microspheres not only implemented a RR behavior on treated surfaces, but they were also capable of enhancing the surface global reflectance up to around 0.4. The angular distribution of the reflected irradiation as assessed in (Castellani et al., 2017) is reported in the Appendix A of the paper (Table A.1). Data used to model the virtual clone of RR materials are presented in this manuscript, while a more complete description of the protocols applied for the characterization, and the characterization results themselves can be found in (Castellani et al., 2017).

These quantities were post-processed to determine the reflection coefficients for the Lambertian diffusively reflected, the specular reflected, and the retro-reflected components, for each incidence angle. The absorption coefficient was always considered equal or higher than 0.6 in accordance with (Castellani et al., 2017). These parameters, which describe the material optical behavior in the numerical model, are reported in Table 1.

It is worthwhile to mention that the investigated RR materials (barium titanate glass microspheres) do not show the highest possible solar reflectance. However, they currently provide the best performance as retroreflectors whithout a significant chromatic alteration of the treated surface . Higher solar reflectance values can be observed in other RR materials, but this happens at the cost of turning the color of the original surface into a metallic tone.

The AS-RR coatings conceptualized in (Manni et al., 2018) showed a selective behavior dependent on the angle of incidence of the solar radiation. Six angular ranges (Fig. 2) were taken into account for the RR layers on vertical and horizontal surfaces. Such surface treatments are expected to behave as retro-reflectors as long as the incident angle falls within the angular range of activation, while present a Lambertian (perfectly diffusive) behavior outside such angular range.

2.2. Step 2: Solar analyses

In *Step 2*, solar analyses were conducted. In addition to the input parameters which were outlined in *Step 1* (i.e. virtual clones of the materials), the boundary conditions (i.e. location, TMY weather file) and the simulation system settings (i.e. number of ambient bounces (ab), number of finite elements (FE), number of events) were considered. The

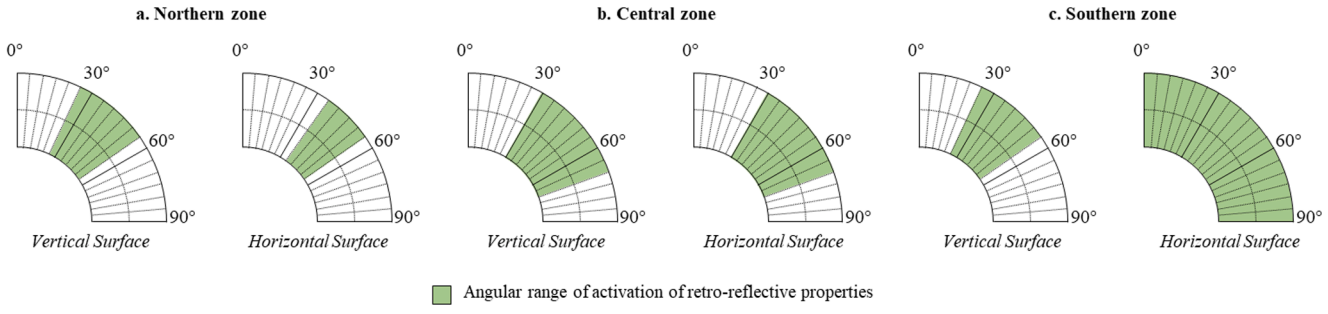

Fig. 2. Angular ranges of activation defined in (Manni et al., 2018) for a horizontal and vertical surface, and for each climate zone.

Table 2
Overview of the input parameters required by the numerical model.

Input data	Symbol	Unit
Urban canyon features		
Height of the building	H	[m]
Width of the street	W	[m]
Height-to-width ratio of UC	H/W	unitless
Orientation of UC	O	[rad]
Surface absorption coefficient	α	[%]
Surface reflection coefficient for the Lambertian diffusively reflected component	ρ_d	[%]
Surface reflection coefficient for the specular reflected component	ρ_s	[%]
Surface reflection coefficient for the retro-reflected component	ρ_{rr}	[%]
Angular ranges to which the defined ρ-value is referred	$\Delta\theta$	[rad]
Boundary conditions		
Global solar irradiation on horizontal surface	$Irr_{glob,hor}$	[W m^{-2}]
Diffuse solar irradiation on horizontal surface	$Irr_{dif,hor}$	[W m^{-2}]
Direct solar irradiation on horizontal surface	$Irr_{dir,hor}$	[W m^{-2}]
Sun azimuth from the north	φ	[rad]
Sun elevation angle	θ	[rad]
Sun altitude	α_{sun}	[rad]
Clearness index	k_t	unitless
Outdoor air temperature	T_{air}	[K]
Relative humidity	Φ	[%]
Simulation variables		
Number of finite elements on a surface	FE	unitless
Number of simulated events	num_events	unitless
Ambient bounces number	ab	unitless

solar analyses were carried out for 15 scenarios, which were assessed for each latitude, and both summer and winter conditions were investigated. The values of the solar irradiation absorbed (Irr_{abs}) by the façades of the two buildings, facing north and south respectively, were estimated with an hourly time step throughout the selected days, which were considered to be representative of the summer and the winter season.

2.2.1. Numerical model and simulation variables

The numerical model to conduct solar analyses is based on a Monte Carlo approach implemented into an on-purpose developed script. The Monte Carlo method was used to estimate the solar irradiation collected by each FE of an urban canyon given the probability that sunrays impinge on a surface – and are consequently absorbed or reflected – according to the input data. A specific energy amount is assigned to each sunray depending on the solar irradiation entering the urban canyon environment and on the number of simulated sunrays. A complete description of both the numerical model and its full-ray tracing routine can be found in a previous paper (Manni et al., 2020a) where the experimental validation of the approach was presented.

Input parameters required by the numerical model with the corresponding symbols and units of measurement are reported in Table 2.

Table 3
Summary of the material patterns which were investigated for each UC geometry.

Investigated scenarios	Applied materials		
	Most irradiated façade	Street ground	Less irradiated façade
Reference case	Brown painting	Asphalt	Brown painting
Case a	Brown painting	RR from the Literature	Brown painting
Case b	Brown painting	Angular-selective RR	Brown painting
Case c	RR from the Literature	Asphalt	Brown painting
Case d	Angular-selective RR	Asphalt	Brown painting

Simulation variables were set to optimize the computational time while maintaining the uncertainty of the results below a 5% threshold. The amount of ambient bounces (i.e. sunrays reflections) considered in the ray-tracing analyses for each sunray before the cutoff was therefore set equal to six. The number of cells in which the UC surfaces are divided (number of FEs on a surface) is determined to guarantee an adequate discretization of the results, and the distance between two consecutive test points was thereofre set to around 1 m. Finally, the number of sunrays entering the UC through the top surface (named "number of events" in the numerical model environment) was set to 10^6 events. These settings allow conducting solar analyses with around 3% uncertainty (Manni et al., 2020a).

2.2.2. Investigated scenarios

Each urban canyon configuration was univocally defined by a combination of aspect ratio, orientation, and material properties. The values for height-to-width ratio adopted were 0.5, 1.0, and 2.0, so that different patterns of urban density such as low-, middle-, and high-density could be investigated. The study focused on assessing the west-east orientation which characterizes the UC with the greatest difference in solar accessibility between the two façades (Manni et al., 2019). The urban canyon geometry was simulated as two-dimensional, i.e. as observed in infinitely long street corridors by setting the the area of analysis in the middle of the UC, where the system is not affected by the boundary effects that take place at the extremes of the UC. The dimensions (reported as building's height by street's width) were 16 m by 8 m in case of a 2.0 H/W, 16 m by 16 m if H/W equaled 1.0, and 16 m by 32 m when H/W was 0.5. The height of the buildings was kept constant throughout the study (Fig. 3).

When it comes to the surface materials, traditional diffuse materials from *Radiance* library were used for the "reference case". Such materials, whose reflection coefficients vary from 0.20 (asphalt) to 0.35 (brown painting), were applied to the urban canyon surfaces. In the "enhanced scenarios", either RR or AS-RR materials were alternatively applied to the most exposed façade (facing south) or to the street ground. In total, up to five cases were analyzed for each UC geometry (Table 3).

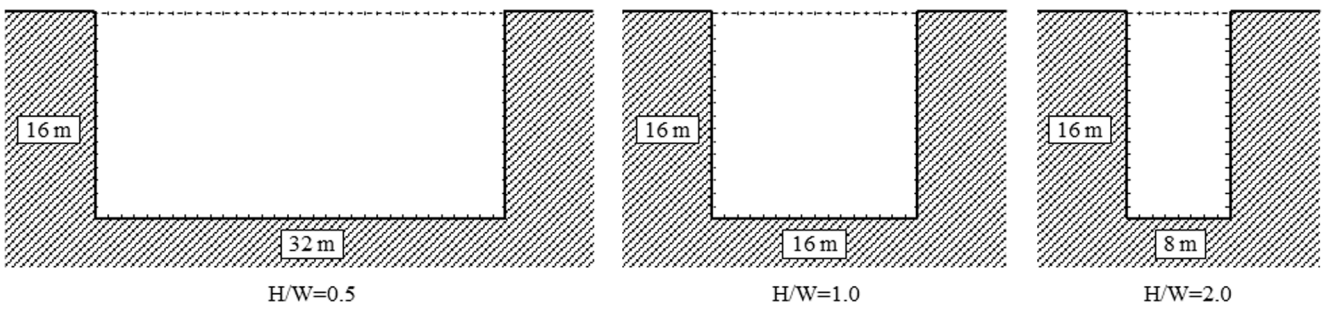

Fig. 3. Geometry configurations of 2D analyzed urban canyon.

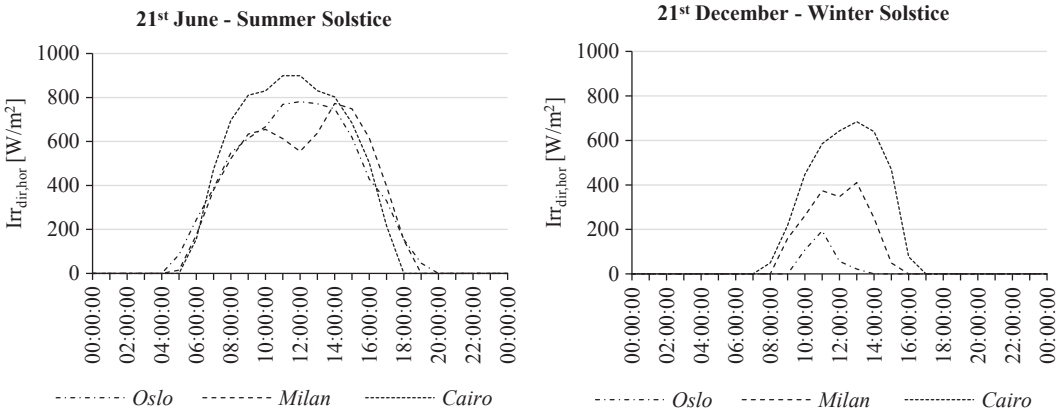

Fig. 4. Hourly distribution of the $Irr_{dir,hor}$ over summer and winter solstices.

Each surface of the UC was considered to have a homogenous reflection coefficient. Through this approach, it was possible to avoid a more detailed level of modelling that includes the positioning of the transparent and opaque parts of the façade. This is coherent with the scope of the proposed approach that focuses on the energy perfromance at urban scale where the architectural and technological appearance of the façades is not detailed, but rather described (in terms of optical properties) with coefficients that regulate the overall behavior.

Three cities representative of different climate zones were chosen as locations to carry out the investigation: Oslo for the northern zone, Milan for the central zone, and Cairo for the southern zone. The 21st of June and the 21st of December were chosen as representative days for the summer and winter conditions, respectively. The duration of the day was determined by the daylight accessibility of an unobstructed horizontal surface, and it varies with the latitude and the season (Fig. 4).

Hence, the hours of the day showing an amount of direct solar irradiation ($Irr_{dir,hor}$) impinging on such a surface which differed from zero were selected. In Oslo, the solar irradiation was assessed from 5:00 a.m. to 7:00 p.m. in summer and from 10:00 a.m. to 1:00 p.m. in winter. Conversely, the number of hours with daylight in Milan and in Cairo were: from 5:00 a.m. to 6:00 p.m. (summer) and from 9:00 a.m. to 3:00 p.m. (winter) in Milan; and from 6:00 a.m. to 5:00 p.m. (summer) and from 8:00 a.m. to 4:00 p.m. (winter) in Cairo.

2.3. Step 3: Data assessment and definition of guidelines

The outcomes of the solar simulations were post-processed in *Step 3* and analysed to identify guidelines for the potential applications of RR and AS-RR coatings to urban surfaces, for the different climate zones.

The weighted variation of absorbed solar irradiation ($\Delta_{\%,wt}$), as defined in Eq. (1) was adopted as main pefromance parameter to assess the perfomrnace in the different scenarios. This quantity represents the difference between the solar irradiation absorbed in the enhanced scenario ($Irr_{abs,enh}$) and the corresponding amount in the reference case ($Irr_{abs,ref}$), over the maximum difference in absorbed solar irradiation registered in the selected *i* urban canyon geometries for the reference case ($max(Irr_{abs,ref,i}) - min(Irr_{abs,ref,i})$). Furthermore, the variation of the absorbed solar irradiation from the reference case ($\Delta_{\%}$) was calculated as reported in Eq. (2).

$$\Delta_{\%,wt} = \frac{Irr_{abs,enh} - Irr_{abs,ref}}{max\left(Irr_{abs,ref,i}\right) - min\left(Irr_{abs,ref,i}\right)} \cdot 100 \quad (1)$$

$$\Delta_{\%} = \frac{Irr_{abs,enh} - Irr_{abs,ref}}{Irr_{abs,ref}} \cdot 100 \quad (2)$$

Both the $\Delta_{\%,wt}$ and the $\Delta_{\%}$ are here used as parameters to evaluate the influences of RR and AS-RR coatings in relation to solar energy gains through buildings' façades.

3. Results and discussion

3.1. Solar accessibility of the façades in the reference case scenario

The outcomes of the solar analyses conducted on the reference cases highlighted that the most irradiated façade facing south was the one in Oslo (summer) and in Cairo (winter), for each aspect ratio. The same was observed for the north-exposed façade. This behavior is due to the variations in the geometry of the sun: in summer, the sunrays were almost parallel to the façade in the Southern zone (hence the Irr_{abs} amount was minor), while in winter were lower above the horizon (worsening mutual shading phenomena in the Northern zone). The greatest Irr_{abs} values for each latitude were observed on the façades overlooking wider UC (H/W = 0.5). The Irr_{abs} on the north and south-exposed façades for each climate zone and aspect ratio, is shown in Fig. 5 (summer) and in

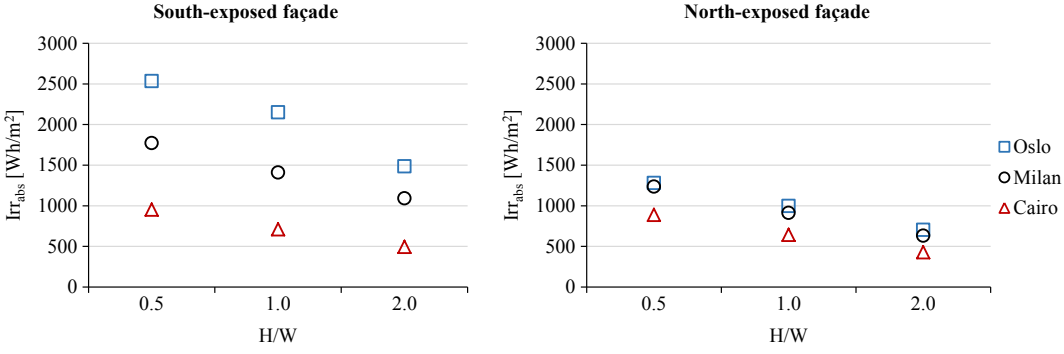

Fig. 5. Irr_{abs} quantities estimated in summer for building façades, depending on latitude and UC aspect ratio.

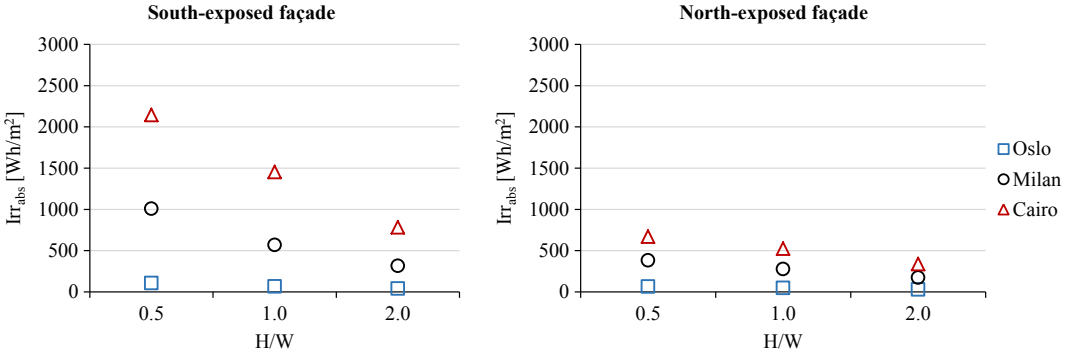

Fig. 6. Irr_{abs} quantities estimated in winter for building façades during winter, depending on latitude and UC ratio.

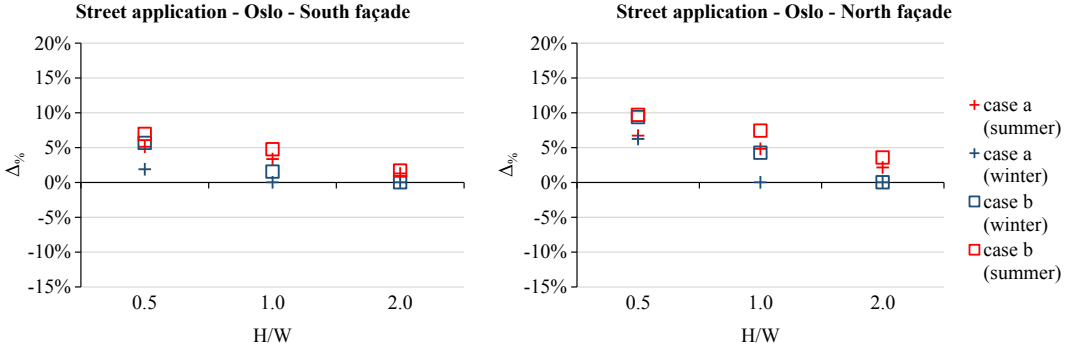

Fig. 7. Estimated $\Delta_{\%}$ values when RR (case a) or AS-RR (case b) materials are applied to the street, in the Northern zone.

Table 4
Calculated amounts of Irr_{abs} by building façades and corresponding $\Delta_{\%}$ and $\Delta_{\%,wt}$ values for all the modelled scenarios in the Northern zone.

			Reference	*Case a*			*Case b*			*Case c*			*Case d*		
			Irr_{abs} [Wh/m²]	Irr_{abs} [Wh/m²]	$\Delta_{\%}$	$\Delta_{\%,wt}$	Irr_{abs} [Wh/m²]	$\Delta_{\%}$	$\Delta_{\%,wt}$	Irr_{abs} [Wh/m²]	$\Delta_{\%}$	$\Delta_{\%,wt}$	Irr_{abs} [Wh/m²]	$\Delta_{\%}$	$\Delta_{\%,wt}$
South Façade	H/W = 0.5	Summer	2535	2665	5%	12%	2710	7%	17%	2340	−8%	−19%	2335	−8%	−19%
		Winter	105	110	2%	3%	110	6%	9%	100	−6%	−9%	100	−6%	−9%
	H/W = 1.0	Summer	2150	2220	3%	7%	2250	5%	10%	1970	−8%	−17%	1975	−8%	−16%
		Winter	65	65	–	–	65	2%	1%	60	−6%	−6%	60	−8%	−7%
	H/W = 2.0	Summer	1485	1505	1%	2%	1510	2%	2%	1350	−9%	−13%	1365	−8%	−11%
		Winter	40	40	–	–	40	–	–	35	−8%	−4%	35	−8%	−4%
North Façade	H/W = 0.5	Summer	1280	1365	7%	15%	1405	10%	21%	1240	−3%	−7%	1265	−1%	−3%
		Winter	65	70	6%	11%	70	9%	17%	65	–	–	65	–	–
	H/W = 1.0	Summer	995	1045	5%	8%	1070	7%	13%	925	−7%	−12%	975	−2%	−4%
		Winter	45	45	–	–	50	4%	6%	45	−6%	−8%	45	–	–
	H/W = 2.0	Summer	700	715	2%	3%	725	4%	4%	625	−11%	−13%	685	−2%	−3%
		Winter	30	30	–	–	30	–	–	25	−4%	−3%	30	–	–

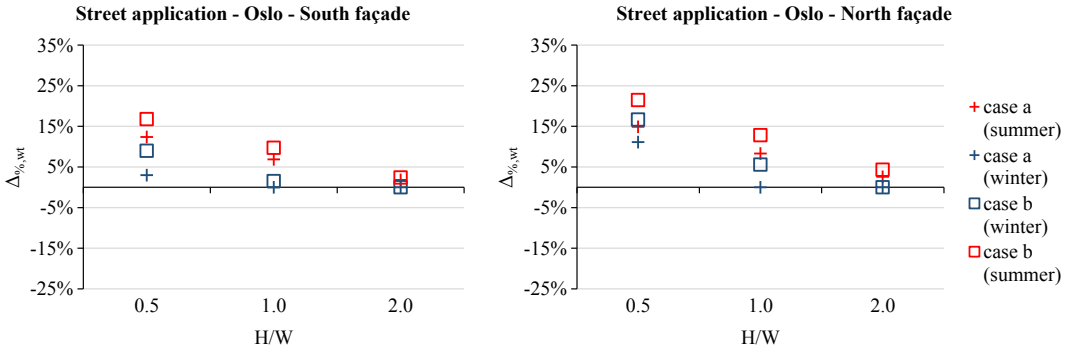

Fig. 8. Estimated $\Delta_{\%,wt}$ values when RR (*case a*) or AS-RR (*case b*) materials are applied to the street, in the Northern zone.

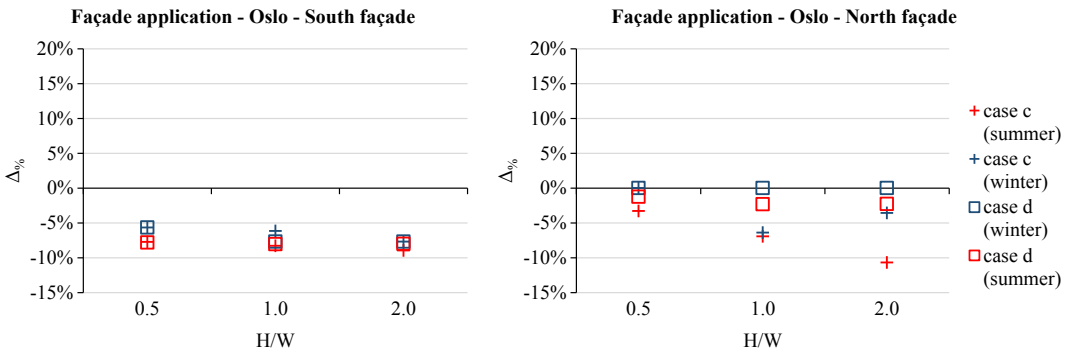

Fig. 9. Estimated $\Delta_{\%}$ values when RR (*case c*) or AS-RR (*case d*) materials are applied to the most irradiated façade, in the Northern zone.

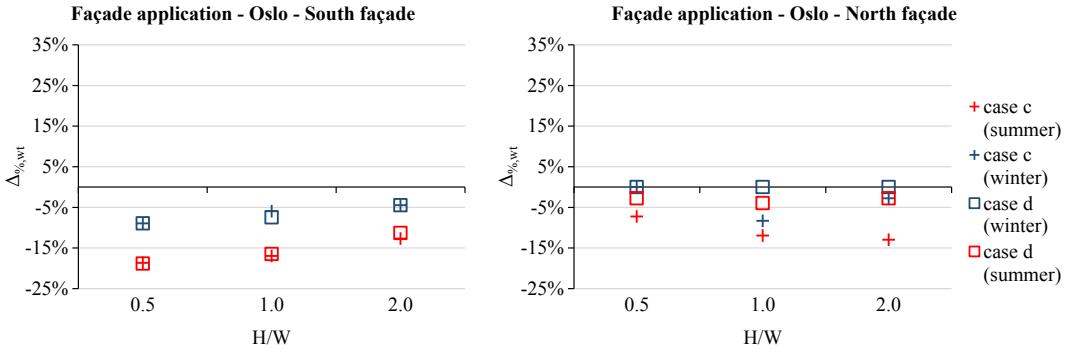

Fig. 10. Estimated $\Delta_{\%,wt}$ values when RR (*case c*) or AS-RR (*case d*) materials are applied to the most irradiated façade, in the Northern zone.

Fig. 6 (winter).

3.2. Influences of optimized cool materials on urban surfaces energy balance

3.2.1. Northern zone

Retro-reflective (*case a*) or angular-selective retro-reflective layers (*case b*) added to the street surface permitted to improve the solar accessibility of the façades (Fig. 7 and Table 4). In summer, the Irr_{abs} on the south-exposed façade is increased from 1% (H/W = 2.0) to 5% (H/W = 0.5) for *case a*, and from 2% (H/W = 2.0) to 7% (H/W = 0.5) for *case b*. Similarly, the Irr_{abs} on the opposite façade showed an increment from 2% (H/W = 2.0) to 7% (H/W = 0.5) for *case a*, and from 4% (H/W = 2.0) to 10% (H/W = 0.5) for *case b*. In winter, the influences of the cool street surface were negligible in the high-density configuration (H/W = 2.0) for both *case a* and *case b*. However, in the UC characterized by H/W = 0.5, AS-RR materials (*case b*) were capable to increase the Irr_{abs} on the north-exposed façade by up to 9%, while RR materials (*case a*) only achieved an increment of 6%.

The data reported in Fig. 8 highlighted that enhancements due to the variation in the material's pattern barely achieve the 20% (in summer, H/W = 0.5) of the maximum improvement of Irr_{abs} achieved through the change of the urban density. Furthermore, the trend of $\Delta_{\%,wt}$ values was the same as the the $\Delta_{\%}$ amounts.

For *case c* and *case d* (RR and AS-RR materials applied to the south-exposed façade), the solar accessibility of the buildings was worsened in summer, and unaltered in winter (Table 4). In summer, the Irr_{abs} on the façade facing south is reduced by 8% from the reference case in all the assessed configurations (Fig. 9). In winter, this percentage varies from −6% to −8% in both *case c* and *case d*, with the higest changes in narrow UC (H/W = 2.0). The influences of RR materials (*case c*) on the north facing façade were more evident for H/W = 2.0 (high urban density): in summer, the Irr_{abs} was lowered by 11%. On the contrary, AS-RR coating (*case d*) barely achieved a 2% reduction in summer. In winter, no variation was observed for *case d* geometries, while the middle-density urban canyon (H/W = 1.0) of *case c* showed a reduction of 6% of Irr_{abs}.

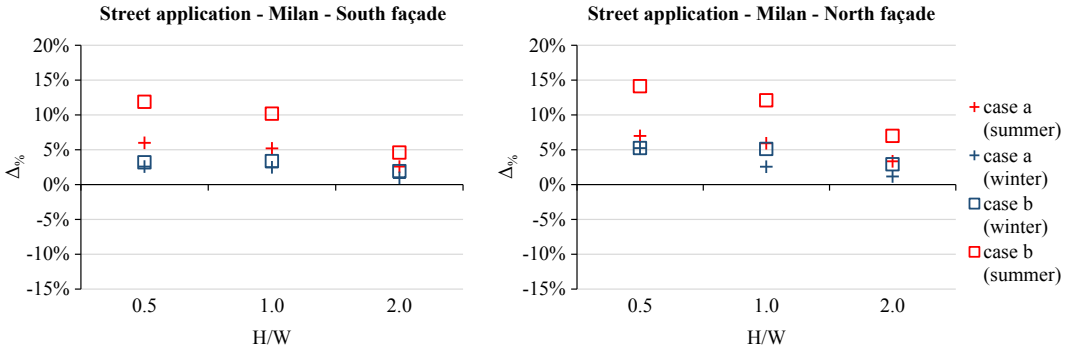

Fig. 11. Estimated $\Delta_{\%}$ values when RR (case a) or AS-RR (case b) materials are applied to the street, in the Central zone.

Table 5
Calculated amounts of Irr_{abs} by building façades and corresponding $\Delta_{\%}$ and $\Delta_{\%,wt}$ values for all the modelled scenarios in the Central zone.

			Reference	Case a			Case b			Case c			Case d		
			Irr_{abs} [Wh/m^2]	Irr_{abs} [Wh/m^2]	$\Delta_{\%}$	$\Delta_{\%,wt}$	Irr_{abs} [Wh/m^2]	$\Delta_{\%}$	$\Delta_{\%,wt}$	Irr_{abs} [Wh/m^2]	$\Delta_{\%}$	$\Delta_{\%,wt}$	Irr_{abs} [Wh/m^2]	$\Delta_{\%}$	$\Delta_{\%,wt}$
South Façade	H/W = 0.5	Summer	1770	1875	6%	16%	1980	12%	31%	1630	−8%	−20%	1630	−8%	−21%
		Winter	1.010	1035	3%	4%	1040	3%	5%	930	−8%	−11%	935	−7%	−11%
	H/W = 1.0	Summer	1410	1480	5%	11%	1550	10%	21%	1300	−8%	−16%	1300	−8%	−16%
		Winter	570	580	2%	2%	585	3%	3%	525	−8%	−6%	525	−7%	−6%
	H/W = 2.0	Summer	1090	1120	3%	4%	1140	5%	7%	995	−9%	−14%	1000	−8%	−13%
		Winter	315	320	1%	–	320	2%	1%	285	−9%	−4%	290	−8%	−4%
North Façade	H/W = 0.5	Summer	1235	1320	7%	14%	1410	14%	29%	1215	−1%	−3%	1225	−1%	−1%
		Winter	380	400	5%	10%	400	5%	10%	370	−3%	−6%	385	1%	2%
	H/W = 1.0	Summer	910	965	6%	9%	1020	12%	18%	870	−4%	−6%	890	−3%	−4%
		Winter	275	280	3%	3%	290	5%	7%	265	−4%	−6%	280	2%	2%
	H/W = 2.0	Summer	630	650	3%	3%	675	7%	7%	575	−9%	−9%	595	−6%	−6%
		Winter	175	175	1%	1%	180	3%	2%	165	−6%	−5%	175	1%	1%

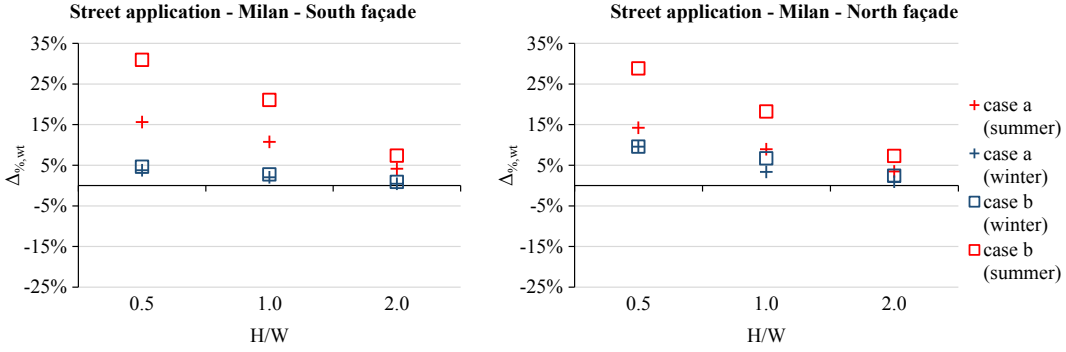

Fig. 12. Estimated $\Delta_{\%,wt}$ values when RR (case a) or AS-RR (case b) materials are applied to the street, in the Central zone.

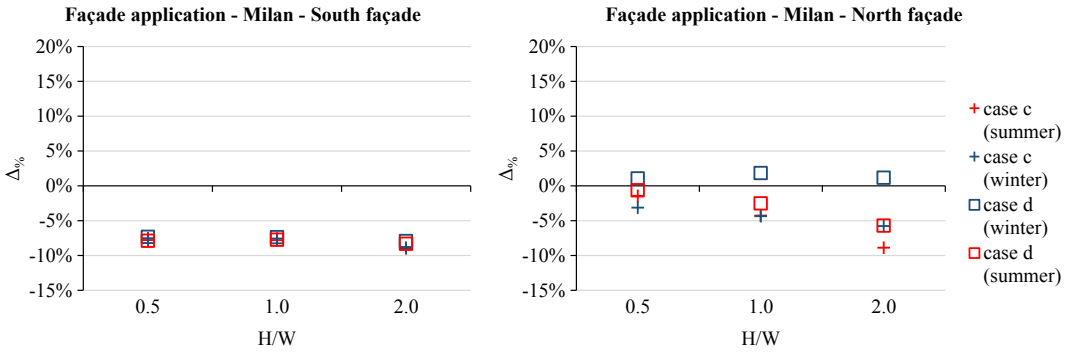

Fig. 13. Estimated $\Delta_{\%}$ values when retro-reflective (case c) or AS-RR (case d) materials are applied to the most irradiated façade, in the Central zone.

Percent changes weighted according to the highest variation in solar gains due to the geometrical pattern showed that RR and AS-RR materials caused up to 20% of reduction in the south-exposed façade when H/W equal to 0.5 (low urban density), and up to 13% reduction with H/W equal to 2.0 (high urban density) (Fig. 10). The $\Delta_{\%,wt}$ values confirmed that Irr_{abs} in winter by the façade facing north was unchanged from the reference case when AS-RR materials were exploited instead of the RR materials.

3.2.2. Central zone

The application of the optimized cool materials (*case a* and *case b*) on the street surface contributed to boosting the solar accessibility of the two façades (Fig. 11 and Table 5). In summer, the Irr_{abs} calculated for the south-exposed façade was increased by a percentage ranging from 3% (H/W = 2.0) to 6% (H/W = 0.5) for *case a* and from 5% (H/W = 2.0) to 12% (H/W = 0.5) for *case b*, respectively. In winter the increments were lower than 3% in all investigated scenarios, with minimum quantities observed with H/W equal to 2.0 (high urban density). In summer, the same trends were observed in the distribution of the percent variation values (even if slightly increased) concerning the opposite façade. In winter, the Irr_{abs} quantities were increased from 1% to 5% for *case a* and from 3% to 5% for *case b*.

The results about $\Delta_{\%,wt}$ highlighted that enhancing the material pattern could cause an increment equal to 15% (*case a*) and to 30% (*case b*) of the greatest variation of Irr_{abs} due to the geometry alteration, on both façades in summer (Fig. 12). In winter, such percent changes did not reach the 5% threshold on the south façade, while they were higher on the opposite façade with H/W equal to 0.5 and to 1.0.

Regarding the application on the south facing façade, RR and AS-RR materials reduced solar energy gains in summer and in winter (Fig. 13

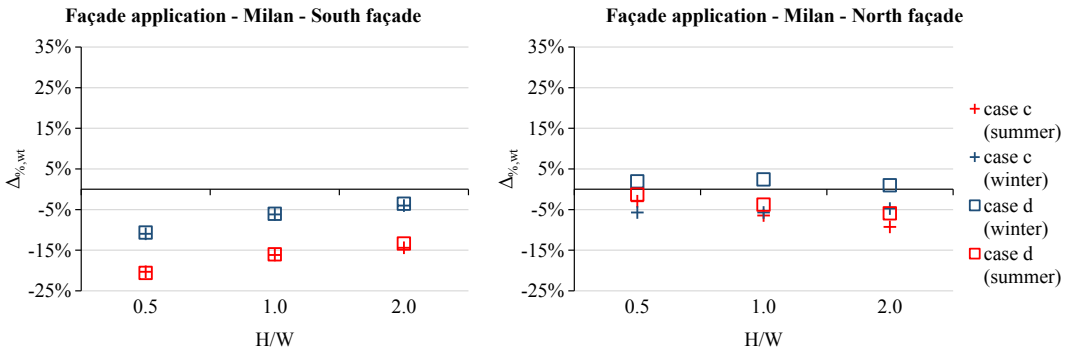

Fig. 14. Estimated $\Delta_{\%,wt}$ values when RR (case c) or AS-RR (case d) materials are applied to the most irradiated façade, in the Central zone.

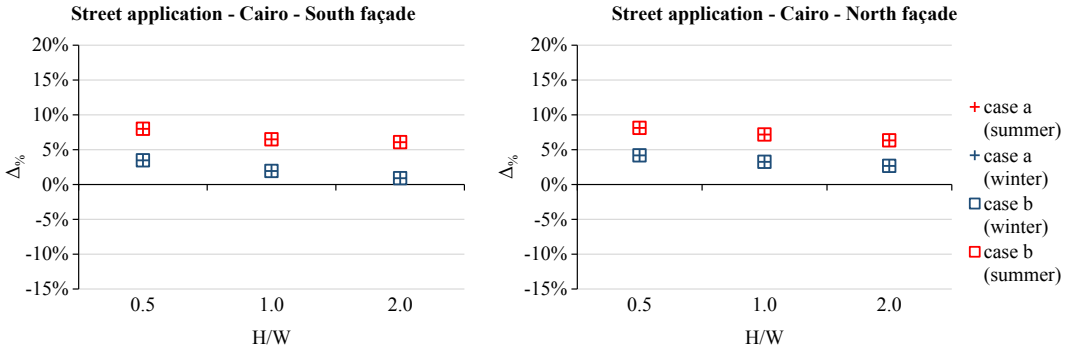

Fig. 15. Estimated $\Delta_{\%}$ values when RR (case a) or AS-RR (case b) materials are applied to the street, in the Southern zone.

Table 6
Calculated amounts of Irr_{abs} by building façades and corresponding $\Delta_{\%}$ and $\Delta_{\%,wt}$ values for all the modelled scenarios in the Southern zone.

			Reference	Case a			Case b			Case c			Case d		
			Irr_{abs} [Wh/m^2]	Irr_{abs} [Wh/m^2]	$\Delta_{\%}$	$\Delta_{\%,wt}$	Irr_{abs} [Wh/m^2]	$\Delta_{\%}$	$\Delta_{\%,wt}$	Irr_{abs} [Wh/m^2]	$\Delta_{\%}$	$\Delta_{\%,wt}$	Irr_{abs} [Wh/m^2]	$\Delta_{\%}$	$\Delta_{\%,wt}$
South Façade	H/W = 0.5	Summer	950	1030	8%	17%	1030	8%	17%	880	−8%	−16%	880	−8%	−16%
		Winter	2145	2220	3%	5%	2220	3%	5%	1985	−7%	−12%	1980	−8%	−12%
	H/W = 1.0	Summer	710	755	6%	10%	755	6%	10%	655	−8%	−12%	660	−7%	−11%
		Winter	1450	1480	2%	2%	1480	2%	2%	1335	−8%	−9%	1340	−8%	−8%
	H/W = 2.0	Summer	495	525	6%	7%	525	6%	7%	460	−7%	−8%	460	−7%	−8%
		Winter	780	790	1%	1%	790	1%	1%	715	−9%	−5%	720	−8%	−5%
North Façade	H/W = 0.5	Summer	890	960	8%	16%	960	8%	16%	890	–	–	890	–	1%
		Winter	670	700	4%	8%	700	4%	8%	620	−7%	−14%	630	−6%	−12%
	H/W = 1.0	Summer	640	690	7%	10%	690	7%	10%	640	–	–	650	1%	2%
		Winter	525	540	3%	5%	540	3%	5%	485	−8%	−12%	490	−7%	−11%
	H/W = 2.0	Summer	425	455	6%	6%	455	6%	6%	430	–	–	440	3%	3%
		Winter	335	845	3%	3%	845	3%	3%	310	−9%	−9%	315	−6%	−6%

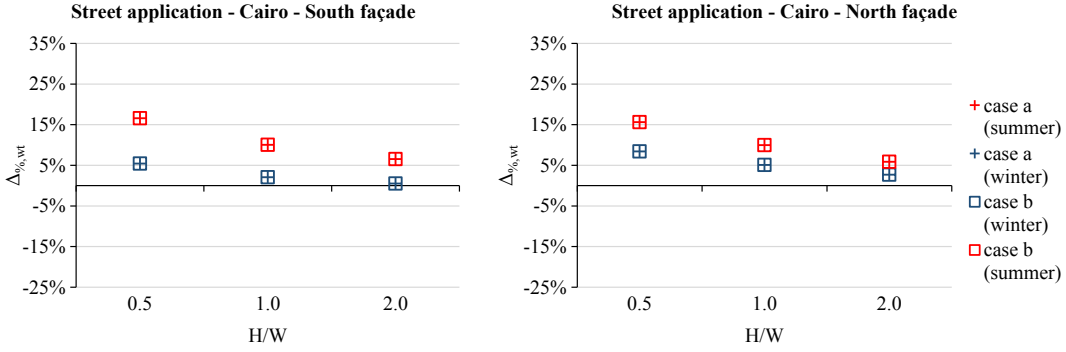

Fig. 16. Estimated $\Delta_{\%,wt}$ values when RR (case a) or AS-RR (case b) materials are applied to the street, in the Southern zone.

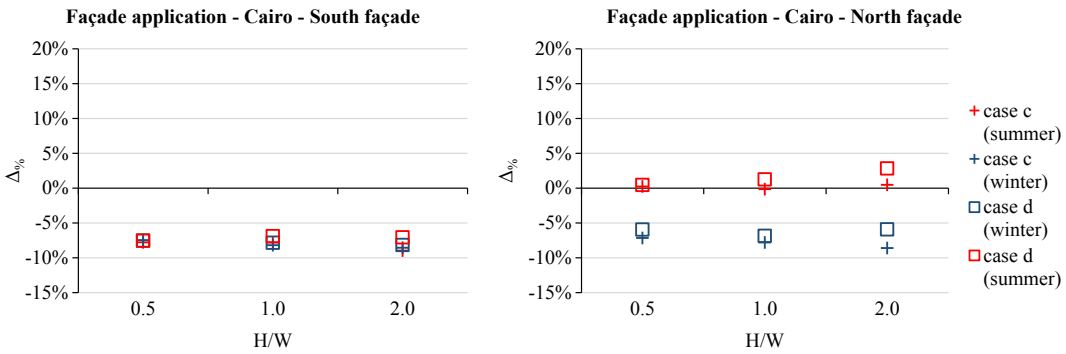

Fig. 17. Estimated $\Delta_{\%}$ values when RR (case c) or AS-RR (case d) materials are applied to the most irradiated façade, in the Southern zone.

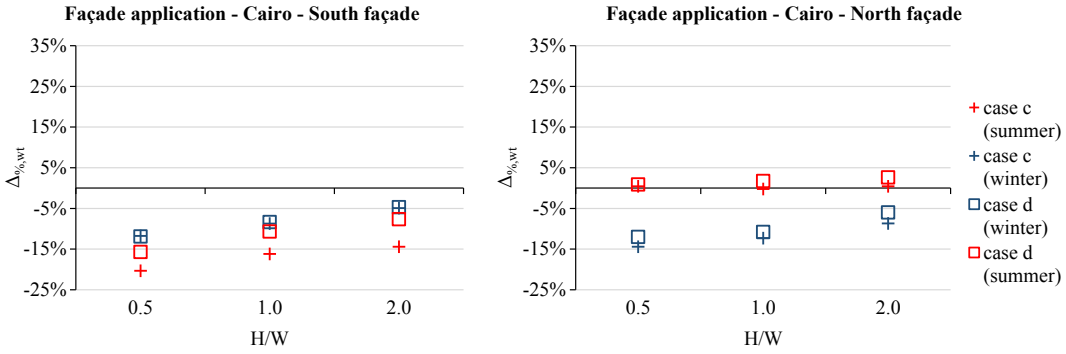

Fig. 18. Estimated $\Delta_{\%,wt}$ values when RR (case c) or AS-RR (case d) materials are applied to the most irradiated façade, in the Southern zone.

and Table 5). The estimated $\Delta_{\%}$ values characterizing the south façade in *case c* and in *case d* were constant and equal to around −8% in summer and in winter throughout the investigated UCs. In the north-exposed façade, RR surface treatments showed higher percent values in winter than in summer when the H/W is equal to 0.5 or 1.0 (low and medium urban density, respectively). Conversely, AS-RR treatments allowed reducing Irr_{abs} by up to 6% (H/W = 2.0) in summer, while increasing by a maximum of 2% in winter (H/W = 1.0).

Distribution of $\Delta_{\%,wt}$ values for the south façade showed some differences in the impact of RR and AS-RR materials between summer and winter (Fig. 14). The investigated surface treatments were responsible for the Irr_{abs} reduction more in summer than in winter, and they resulted to be more effective in wider street corridors (H/W = 0.5). Regarding the north-exposed façade, $\Delta_{\%,wt}$ values were as high as the $\Delta_{\%}$, except for the quantities referring to *case c* in winter whose distribution turned out to be flattened around the −6% share.

3.2.3. Southern zone

The angular range of activation of RR properties which was defined in (Manni et al., 2018) for the horizontal surfaces (i.e. street application) in the Southern zone ranged from 0° to 90° for the *case a* and the *case b*. In both cases, the solar accessibility of the south-exposed façade was increased from 6% (H/W = 2.0) to 8% (H/W = 0.5) in summer, while in winter the values varied between 1% (H/W = 2.0) and 3% (H/W = 0.5) (Fig. 15 and Table 6). The same shares were observed on the opposite façade (north oriented) in summer; while they turned out to be slightly increased in winter (around 2% higher than south façade).

The estimated $\Delta_{\%,wt}$ values highlighted that cool materials applied on the street played a significant role in increasing the solar irradiation absorbed by the façades when wider UC were considered by guaranteeing a percent variation up to 17% of the maximum increment due to geometry (Fig. 16).

Regarding the application of RR and AS-RR materials on the façade, solar energy gains on the south-exposed façade were reduced throughout the year, while the opposite façade was only mitigated in winter (Fig. 17 and Table 6). The $\Delta_{\%}$ quantities calculated for the south-exposed façade in *case c* and *case d* were distributed around the −8% value. The north façade was characterized by a reduction in the $Irr_{abs,win}$ equal to 6% for both *case c* and *case d*. In summer, the solar accessibility of the façade was increased by up to 3% (H/W = 2.0) with the application of AS-RR materials.

The Fig. 18 showed how the $\Delta_{\%,wt}$ distribution of south façade ranges between −20% and −14% for *case c*, and between −16% and −8% for *case d*, in summer; while in winter, the distribution of the values from the two case studies coincided. In winter, the reduction on the opposite façade was mostly affected by the selected material pattern with H/W equal to 0.5, while in summer such reduction barely achieved the 3%.

3.3. Guidelines for the application of optimized cool materials

The outcomes of this study showed that RR and AS-RR materials always increased the solar irradiation absorbed by the two façades of the UC, when they were simulated as surface treatments for the street surface. The higher solar reflectance value characterizing the street (if compared to the asphalt from the reference case) played a significant role in this behaviour. The magnitude of the phenomenon was found to be inversely proportional to the aspect ratio, and the investigated cool coatings showed a greater impact in the Central zone, while being barely

effective in the Southern zone.

The following guidelines can be carried out for the street application:

- RR and AS-RR materials can be applied to the street in order to increase the solar irradiation absorbed by the two façades (greatest variations were observed in scenarios enhanced with AS-RR materials);
- Effectiveness of both RR and AS-RR materials is higher in summer than in winter;
- RR and AS-RR materials applied to the street surface achieve higher performance levels in low-density ($H/W \leq 0.5$) urban environment.

Optimized cool materials on the south elevation reduced the solar irradiation absorbed by this façade throughout the year. The estimated variation from the reference case assumed values close to −8% in every scenario. Conversely, on the opposite façade, the influences of the coating were mitigated by using AS-RR materials instead of RR ones. Furthermore, the absorbed irradiation was reduced more in summer than in winter in the Northern and Central zones, while the opposite tendency was observed in the Southern zone.

The following guidelines can be carried out for the façade application:

- RR and AS-RR materials can always be applied to the south-exposed façade to reduce the irradiation absorbed by this surface;
- Effectiveness of RR and AS-RR materials is higher in summer than in winter, when the Northern and Central zones are considered;
- RR and AS-RR materials showed higher performance levels on high-density ($H/W \geq 2.0$) urban environment.

3.4. Limitations

The study reported in this paper presents two main limitations. Firstly, the research activities only focused on short-wave energy exchanges within the UC and between the UC and the surrounding environment, without linking solar gains within the possible overheating of the urban canyon. Therefore, the impacts of urban coatings on the energy balance is just partially assessed. However, using the variation in absorbed solar irradiation as the main output parameter (instead of variations in air temperature) to evaluate RR and AS-RR materials may also represented a strength of this study. The analysis of the Irr_{abs} allowed more general conclusions to be taken on the effectiveness of these materials in different climate conditions without investigating the entire thermal domain of the canyon. Since the thermal domain of the UC depends on so many other variables (i.e. wind speed, humidity, air temperature), comprehensive investigation with such approach would be impossible in practical terms.

Secondly, the utilization of data about solar irradiation from statistic-based weather data files may result in incorrect computing of diffuse fractions as well as in systematic error within the evaluation of the potential benefits. Such type of weather data files is however the usual source of weather data at the preliminary phase of the design process, and are today the most used and accepted sources for input data in the design process based on building performance simulation.

4. Conclusions and future developments

Different effects were observed depending on the surfaces where RR and AS-RR materials were exploited. When applied to the street, such surface treatments were capable of increasing the solar irradiation absorbed by both the building façades (more in summer than in winter) with greater variations on the north-facing façade than on the south-facing façade. Implementing an angular-selective behavior led to increasing the estimated percent variations from the reference case. The exploitation of RR materials on the south façade caused a reduction of the absorbed solar irradiation: the magnitude of this phenomenon depends, in the north façade, on the geometry (i.e. H/W, orientation) of the UC . Angular ranges of activation of the RR properties demonstrated to be effective in reducing the mitigation potential of RR materials during the winter season in the Northern and Central zones while during summer in the Southern zone.

The findings of this study demonstrate that:

- RR and AS-RR applied on the street surfaces affect the solar irradiation absorbed by the two façades at the same way, although with different magnitudes;
- In their best street application (low-density UC in Milan, Central zone), optimized cool materials can increase the Irr_{abs} by façades both in summer (around 13%) and in winter (around 4%) compared to a reference, conventional configuration;
- RR and AS-RR materials applied to the south façade always reduce by around 8% the irradiation absorbed by the same façade;
- In their best façade application (high-density UC in Milan, Central zone), optimized cool materials can reduce by 8% the Irr_{abs} by south façade throughout the year, while lowering by 6% Irr_{abs} by the other façade in summer with negligible effects in winter.

In conclusion, this investigation assessed cool materials to be effective technologies to enhance the solar accessibility of buildings' façades within street corridors while reducing the risk of the unwanted UHI. However, further analyses are needed in order to investigate the comprehensive effects of such materials by considering other parameters such as the amounts of solar irradiation that are reflected outside the canyon boundaries.

The future developments of this research may also concern:

- The enhancement of the Monte Carlo-based numerical model by including other energy exchange phenomena in the calculation routines, such as long-wave radiative heat exhanges and convective heat exchanges.
- The application of the current version of the numerical model to investigate visual comfort issues (e.g. glare) due to HR and RR materials.
- The further optimization of the angular ranges of activation of the RR properties.
- The assessment of the performance for the case of RR materials with enhanced solar reflectance.

Declaration of Competing Interest

The authors declared that there is no conflict of interest.

Acknowledgments

The authors wish to thank the Norwegian University of Science and Technology (Trondheim, Norway), the University of Perugia (Perugia, Italy) and the CIRIAF – Interuniversity Research Center on Pollution and Environment "Mauro Felli" for having supported the collaboration between the two universities in this work, framed in the EU programme for education, training, youth and sport – 'ERASMUS+'.

Appendix A

See Table A1.

Table A1
Percentage angular distribution of the reflected radiation for eight angles of incidence of the sunray (Castellani et al., 2017).

Direction of reflected light	Angle of incidence							
	0°	10°	20°	30°	40°	50°	60°	70°
−80°	1	1	1	1	1	1	1	2
−70°	2	2	2	2	2	2	4	5
−60°	3	3	3	3	3	3	4	4
−50°	5	5	4	4	5	4	5	6
−40°	5	6	4	4	5	3	3	3
−30°	7	8	7	7	8	6	5	4
−20°	8	9	6	6	7	4	3	3
−10°	10	10	6	6	8	4	2	3
0°	**15**	9	6	6	7	3	2	2
10°	10	**15**	17	12	8	10	5	8
20°	8	10	**17**	12	8	10	5	8
30°	7	9	12	**17**	13	11	9	6
40°	7	6	8	11	**13**	11	8	5
50°	5	3	5	5	5	**15**	14	9
60	5	3	5	5	5	10	**19**	9
70°	1	1	2	2	2	4	8	**21**
80°	1	1	1	1	1	1	2	5

References

Battista, G., de Lieto Vollaro, R., Zinzi, M., 2019. Assessment of urban overheating mitigation strategies in a square in Rome, Italy. Sol. Energy 180, 608–621. https://doi.org/10.1016/j.solener.2019.01.074.

Castellani, B., Morini, E., Anderini, E., Filipponi, M., Rossi, F., 2017. Development and characterization of retro-reflective colored tiles for advanced building skins. Energy Build. 154, 513–522. https://doi.org/10.1016/j.enbuild.2017.08.078.

Grilo, F., Pinho, P., Aleixo, C., Catita, C., Silva, P., Lopes, N., Freitas, C., Santos-Reis, M., McPhearson, T., Branquinho, C., 2020. Using green to cool the grey: Modelling the cooling effect of green spaces with a high spatial resolution. Sci. Total Environ. 724, 138182 https://doi.org/10.1016/j.scitotenv.2020.138182.

Jandaghian, Z., Berardi, U., 2020. Analysis of the cooling effects of higher albedo surfaces during heat waves coupling the Weather Research and Forecasting model with building energy models. Energy Build. 207, 109627 https://doi.org/10.1016/j.enbuild.2019.109627.

Kousis, I., Fabiani, C., Gobbi, L., Pisello, A.L., 2020. Phosphorescent-based pavements for counteracting urban overheating – A proof of concept. Sol. Energy 202, 540–552. https://doi.org/10.1016/j.solener.2020.03.092.

Liu, N., Morawska, L., 2020. Modeling the urban heat island mitigation effect of cool coatings in realistic urban morphology. J. Clean. Prod. 264, 121560 https://doi.org/10.1016/j.jclepro.2020.121560.

Lobaccaro, G., Acero, J.A., Martinez, G.S., Padro, A., Laburu, T., Fernandez, G., 2019. Effects of orientations, aspect ratios, pavement materials and vegetation elements on thermal stress inside typical urban canyons. Int. J. Environ. Res. Public Health 16, 3574. https://doi.org/10.3390/ijerph16193574.

Lobaccaro, G., Wiberg, A.H., Ceci, G., Manni, M., Lolli, N., Berardi, U., 2018. Parametric design to minimize the embodied GHG emissions in a ZEB. Energy Build. 167 https://doi.org/10.1016/j.enbuild.2018.02.025.

Manni, M., Bonamente, E., Lobaccaro, G., Goia, F., Nicolini, A., Bozonnet, E., Rossi, F., 2020a. Development and validation of a Monte Carlo-based numerical model for solar analyses in urban canyon configurations. Build. Environ. 170, 106638 https://doi.org/10.1016/j.buildenv.2019.106638.

Manni, M., Lobaccaro, G., Goia, F., Nicolini, A., 2018. An inverse approach to identify selective angular properties of retro-reflective materials for urban heat island mitigation. Sol. Energy 176, 194–210. https://doi.org/10.1016/J.SOLENER.2018.10.003.

Manni, M., Lobaccaro, G., Goia, F., Nicolini, A., Rossi, F., 2019. Exploiting selective angular properties of retro-reflective coatings to mitigate solar irradiation within the urban canyon. Sol. Energy 189, 74–85. https://doi.org/10.1016/J.SOLENER.2019.07.045.

Manni, M., Petrozzi, A., Coccia, V., Nicolini, A., Cotana, F., 2020b. Investigating alternative development strategies for sport arenas based on active and passive systems. J. Build. Eng. 31, 101340 https://doi.org/10.1016/j.jobe.2020.101340.

Mauri, L., Battista, G., de Lieto Vollaro, E., de Lieto Vollaro, R., 2018. Retroreflective materials for building's façades: Experimental characterization and numerical simulations. Sol. Energy 171, 150–156. https://doi.org/10.1016/j.solener.2018.06.073.

Nazarian, N., Dumas, N., Kleissl, J., Norford, L., 2019. Effectiveness of cool walls on cooling load and urban temperature in a tropical climate. Energy Build. 187, 144–162. https://doi.org/10.1016/j.enbuild.2019.01.022.

Oke, T.R., 1981. Canyon geometry and the nocturnal urban heat island: Comparison of scale model and field observations. J. Climatol. 1, 237–254. https://doi.org/10.1002/joc.3370010304.

Pantavou, K., Theoharatos, G., Mavrakis, A., Santamouris, M., 2013. Evaluating thermal comfort conditions and health responses during an extremely hot summer in Athens. Build. Environ. https://doi.org/10.1016/j.buildenv.2010.07.026.

Pioppi, B., Pigliautile, I., Piselli, C., Pisello, A.L., 2020. Cultural heritage microclimate change: Human-centric approach to experimentally investigate intra-urban overheating and numerically assess foreseen future scenarios impact. Sci. Total Environ. 703, 134448 https://doi.org/10.1016/j.scitotenv.2019.134448.

Piselli, C., Castaldo, V.L., Pigliautile, I., Pisello, A.L., Cotana, F., 2018. Outdoor comfort conditions in urban areas: On citizens' perspective about microclimate mitigation of urban transit areas. Sustain. Cities Soc. 39, 16–36. https://doi.org/10.1016/J.SCS.2018.02.004.

Piselli, C., Castaldo, V.L., Pisello, A.L., 2019. How to enhance thermal energy storage effect of PCM in roofs with varying solar reflectance: Experimental and numerical assessment of a new roof system for passive cooling in different climate conditions. Sol. Energy 192, 106–119. https://doi.org/10.1016/j.solener.2018.06.047.

Rahman, M.A., Moser, A., Rötzer, T., Pauleit, S., 2017. Microclimatic differences and their influence on transpirational cooling of Tilia cordata in two contrasting street canyons in Munich. Germany. Agric. For. Meteorol. 232, 443–456. https://doi.org/10.1016/J.AGRFORMET.2016.10.006.

Rossi, F., Castellani, B., Presciutti, A., Morini, E., Filipponi, M., Nicolini, A., Santamouris, M., 2015. Retroreflective façades for urban heat island mitigation: Experimental investigation and energy evaluations. Appl. Energy 145, 8–20. https://doi.org/10.1016/j.apenergy.2015.01.129.

Sakai, H., Iyota, H., 2017. Development of two new types of retroreflective materials as countermeasures to urban heat Islands. Int. J. Thermophys. https://doi.org/10.1007/s10765-017-2266-y.

Santamouris, M., Cartalis, C., Synnefa, A., Kolokotsa, D., 2015. On the impact of urban heat island and global warming on the power demand and electricity consumption of buildings - A review. Energy Build. 98, 119–124. https://doi.org/10.1016/j.enbuild.2014.09.052.

Tsoka, S., Theodosiou, T., Tsikaloudaki, K., Flourentzou, F., 2018. Modeling the performance of cool pavements and the effect of their aging on outdoor surface and air temperatures. Sustain. Cities Soc. 42, 276–288. https://doi.org/10.1016/j.scs.2018.07.016.

United Nations, D. of E. and S.A., 2014. World Urbanization Prospects: The 2014 Revision, Highlights.

Vallati, A., Mauri, L., Colucci, C., 2018. Impact of shortwave multiple reflections in an urban street canyon on building thermal energy demands. Energy Build. 174, 77–84. https://doi.org/10.1016/J.ENBUILD.2018.06.037.

Warren, C.M.J., 2014. Heat Islands; Understanding and Mitigating Heat in Urban Areas20122Lisa Gartland. Heat Islands; Understanding and Mitigating Heat in Urban Areas. London: Earthscan 2011. 192 pp., ISBN: 978-1-84971-298-9 $64.95. Prop. Manag. 30, 105–106. https://doi.org/10.1108/pm.2012.30.1.105.2.

Xie, X., Huang, Z., Wang, J., Xie, Z., 2005. The impact of solar radiation and street layout on pollutant dispersion in street canyon. Build. Environ. 40, 201–212. https://doi.org/10.1016/j.buildenv.2004.07.013.

Xu, X., González, J.E., Shen, S., Miao, S., Dou, J., 2018. Impacts of urbanization and air pollution on building energy demands — Beijing case study. Appl. Energy 225, 98–109. https://doi.org/10.1016/J.APENERGY.2018.04.120.

Zhou, D., Zhang, L., Li, D., Huang, D., Zhu, C., 2016. Climate–vegetation control on the diurnal and seasonal variations of surface urban heat islands in China. Environ. Res. Lett. 11 https://doi.org/10.1088/1748-9326/11/7/074009.

Ziaul, S., Pal, S., 2020. Modeling the effects of green alternative on heat island mitigation of a meso level town, West Bengal, India. Adv. Sp. Res. 65, 1789–1802. https://doi.org/10.1016/j.asr.2019.12.031.

Zinzi, M., Carnielo, E., Rossi, G., 2015. Directional and angular response of construction materials solar properties: Characterisation and assessment. Sol. Energy 115, 52–67. https://doi.org/10.1016/j.solener.2015.02.015.